Supplement of Atmos. Chem. Phys., 25, 771–795, 2025
https://doi.org/10.5194/acp-25-771-2025-supplement

Atmospheric Chemistry and Physics
Open Access
EGU

Supplement of

Exploring the processes controlling secondary inorganic aerosol: evaluating the global GEOS-Chem simulation using a suite of aircraft campaigns

Olivia G. Norman et al.

Correspondence to: Olivia G. Norman (onorman@mit.edu) and Colette L. Heald (colette.heald@env.ethz.ch)

Table S1. Complete list of instruments and associated PI for all species data included in this paper across all the campaigns.

	SNA + Cl^-	**HNO_3**	**NH_3**	**SO_2**	**HCl**	**Na^+**
ADRIEX	Hugh Coe (Q-AMS)	-	-	-	-	-
MILAGRO	Jose L. Jimenez (HR-ToF-AMS)	Paul Wennberg, John Crounse (CIT CIMS)	-	Paul Wennberg, John Crounse (CIT CIMS)	-	Rodney Weber (PILS-IC)
EUCAARI	Hugh Coe (C-ToF-AMS)	-	-	-	-	-
CalNex	Ann Middlebrook, Roya Bahreini (C-ToF-AMS)	Andy Neuman, John B. Nowak (CIMS)	John B. Nowak, Andy Neuman (CIMS)	John S Holloway (UV Pulsed Fluorescence)	Greg Huey (GT CIMS)	-
DC3	Jose L. Jimenez (HR-ToF-AMS)	Paul Wennberg, John Crounse (CIT CIMS)	-	Greg Huey (GT CIMS)	-	Jack Dibb (SAGA-AERO)
SENEX	Ann Middlebrook, Jin Liao, Andre Welti (C-ToF-AMS)	Andy Neuman, John B. Nowak (CIMS)	John B. Nowak, Andy Neuman (CIMS)	John S Holloway (UV Pulsed Fluorescence)	-	-
WINTER	Jose L. Jimenez, Pedro Campuzano-Jost (HR-ToF-AMS)	Joel Thornton, Felipe Lopez-Hilfiker (CIMS)	-	Marc N. Fiddler, Jaime R. Green, Solomon Bililign (UV Pulsed Fluorescence)	Joel Thornton, Felipe Lopez-Hilfiker (CIMS)	-
KORUS-AQ	Jose L. Jimenez, Pedro Campuzano-Jost, Benjamin A. Nault (HR-ToF-AMS)	Paul Wennberg, John Crounse, Michelle Kim (CIT CIMS)	-	Greg Huey (GT CIMS)	Greg Huey (GT CIMS)	Jack Dibb (SAGA-AERO)
EMeRGe-EU	Johannes Schneider, Stephan Borrmann, Katharina Kaiser (C-ToF-AMS)	-	-	Hans Schlager, Lisa Eirenschmalz (CIMS)	-	-
EMeRGe-AS	Johannes Schneider, Stephan Borrmann, Katharina Kaiser (C-ToF-AMS)	-	-	Hans Schlager, Lisa Eirenschmalz (CIMS)	-	-
FIREX-AQ	Jose L. Jimenez, Pedro Campuzano-Jost, Benjamin A. Nault (HR-ToF-AMS)	Paul Wennberg, John Crounse, Krystal Vasquez, Lu Xu (CIT CIMS)	-	Andrew Rollins (LIF)	-	Jack Dibb (SAGA-AERO)

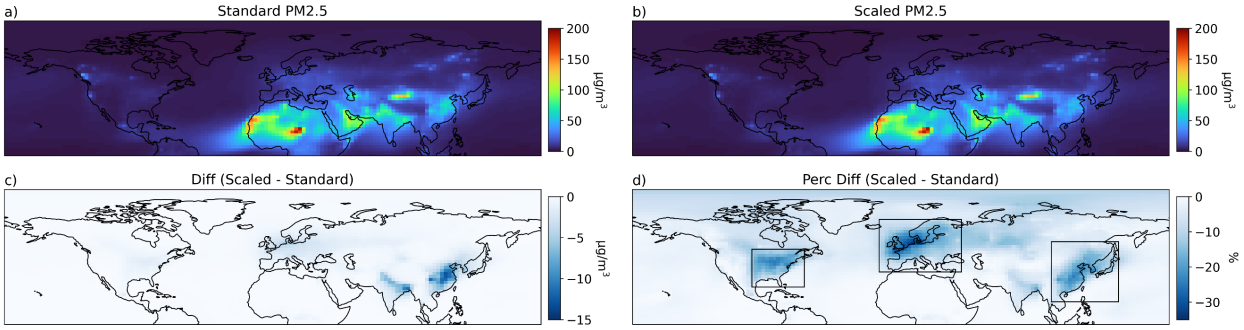

Figure S1. Annual average $PM_{2.5}$ concentrations in the Northern Hemisphere for a) the standard GEOS-Chem simulation and b) for the sensitivity test where NO_3^- is scaled down by a NMB of 1.76. The difference (c) and percent difference (d) between $PM_{2.5}$ concentrations in the scaled and the standard simulation are also shown. Outlined in d) are the three regions with the largest decreases in PM2.5.

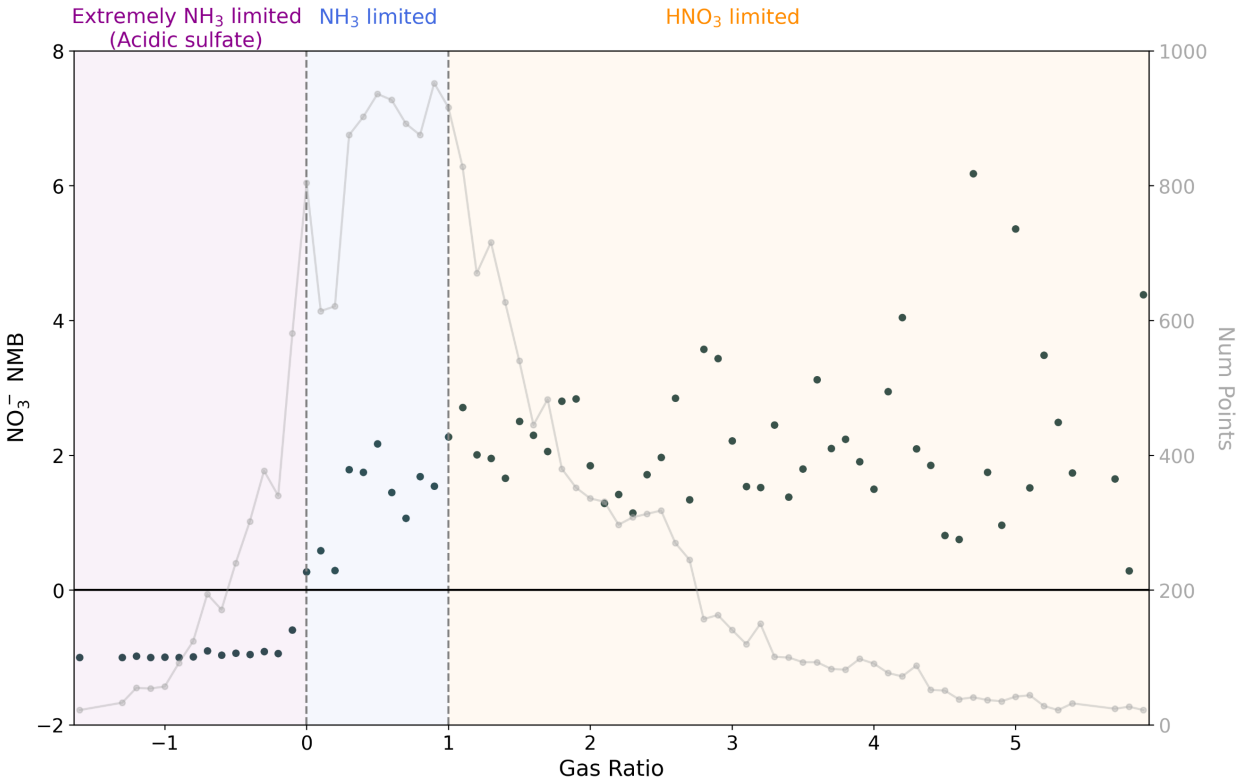

Figure S2. NMB for nitrate concentrations versus gas ratio (points). The number of points in each bin is also shown (line), with bins with less than 20 data points filtered out. The three regimes (extreme NH_3 limitation, NH_3 limitation, and HNO_3 limitation) are indicated.

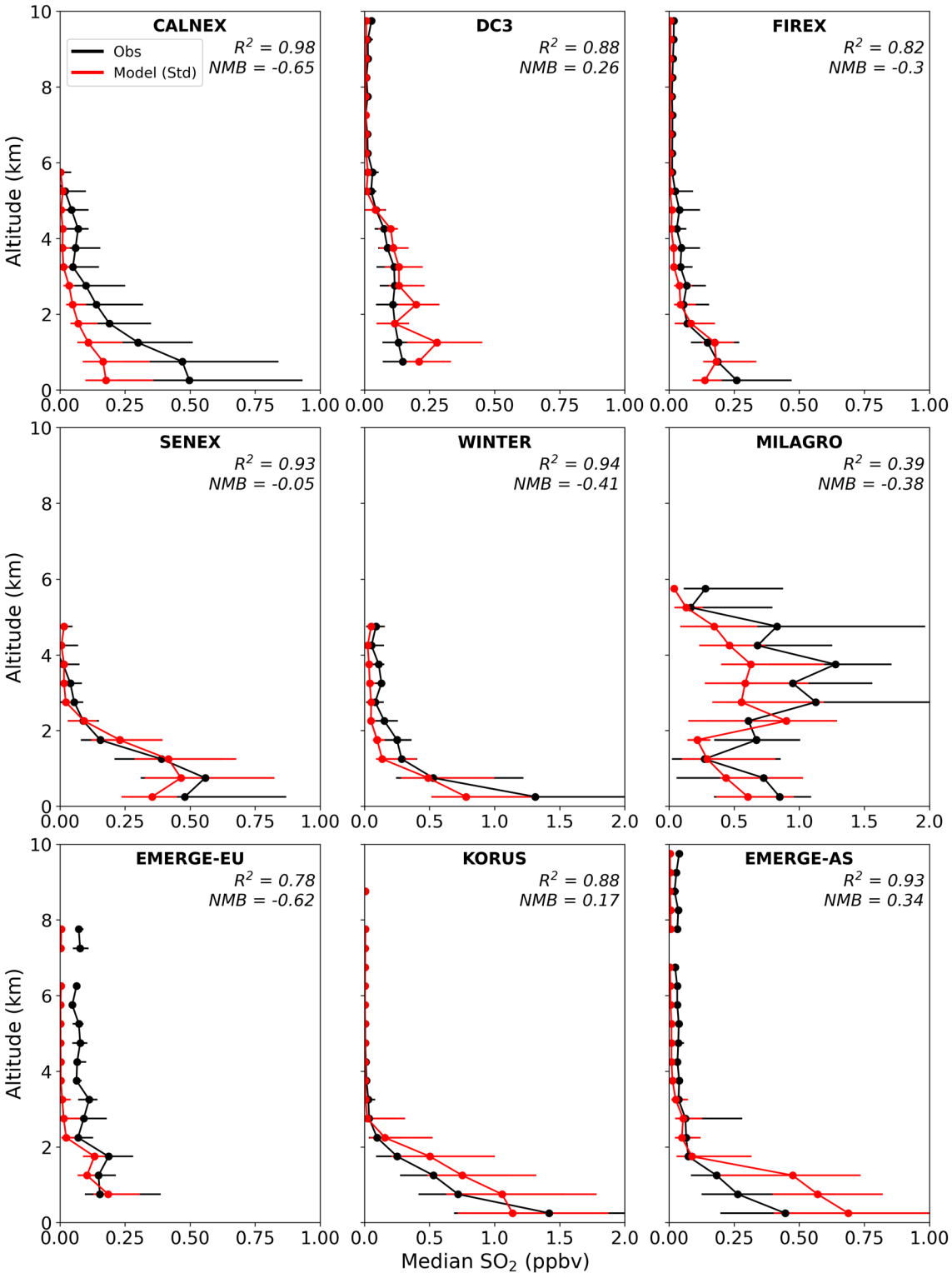

Figure S3. Median vertical profile of observed (black) and simulated (red) SO_2 concentrations. Points are binned to the nearest 0.5 km. Error bars represent the interquartile range (IQR). Altitude bins with less than 10 points per bin are not shown. R^2 and NMB for the vertical variability is also reported for each campaign.

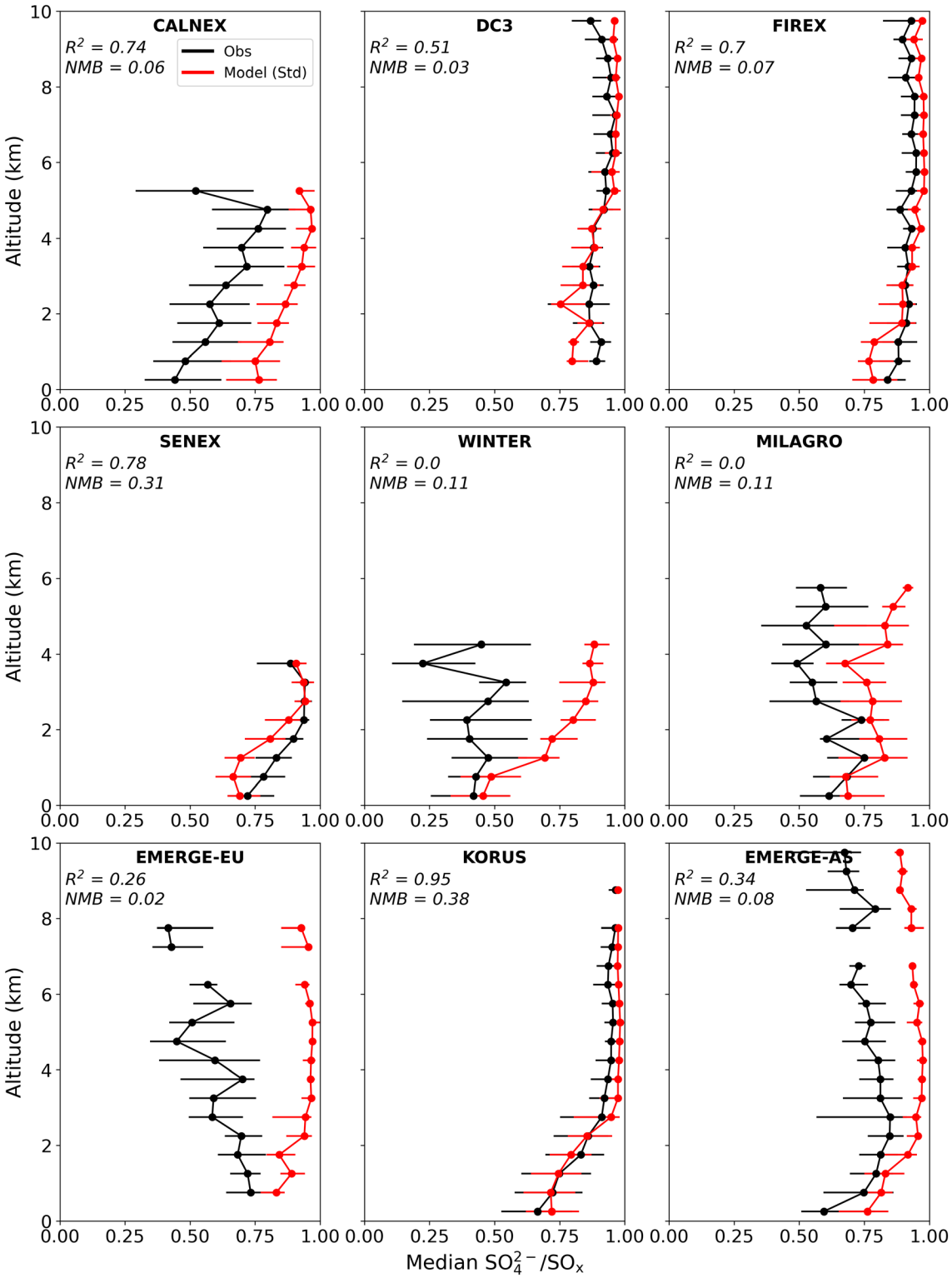

Figure S4. Median vertical profile of observed (black) and simulated (red) of the molar ratio SO_4^{2-}/SO_x. Points are binned to the nearest 0.5 km. Error bars represent the interquartile range (IQR). Altitude bins with less than 10 points per bin are not shown. R^2 and NMB for the vertical variability is also reported for each campaign. Points with missing or negative SO_4^{2-} and SO_2 are removed.

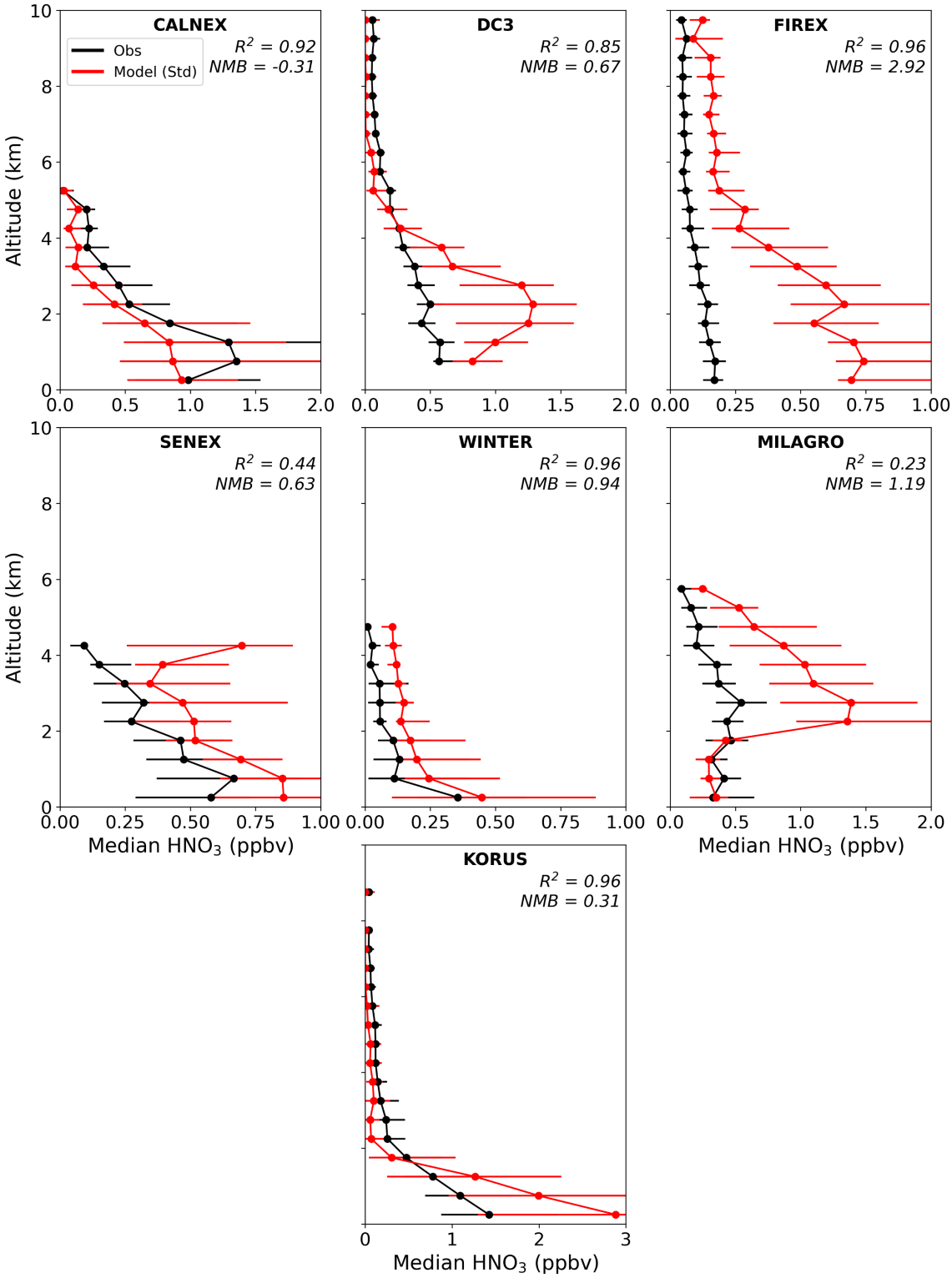

Figure S5. Median vertical profile of observed (black) and simulated (red) HNO_3 concentrations. Points are binned to the nearest 0.5 km. Error bars represent the interquartile range (IQR). Altitude bins with less than 10 points per bin are not shown. R^2 and NMB for the vertical variability is also reported for each campaign.

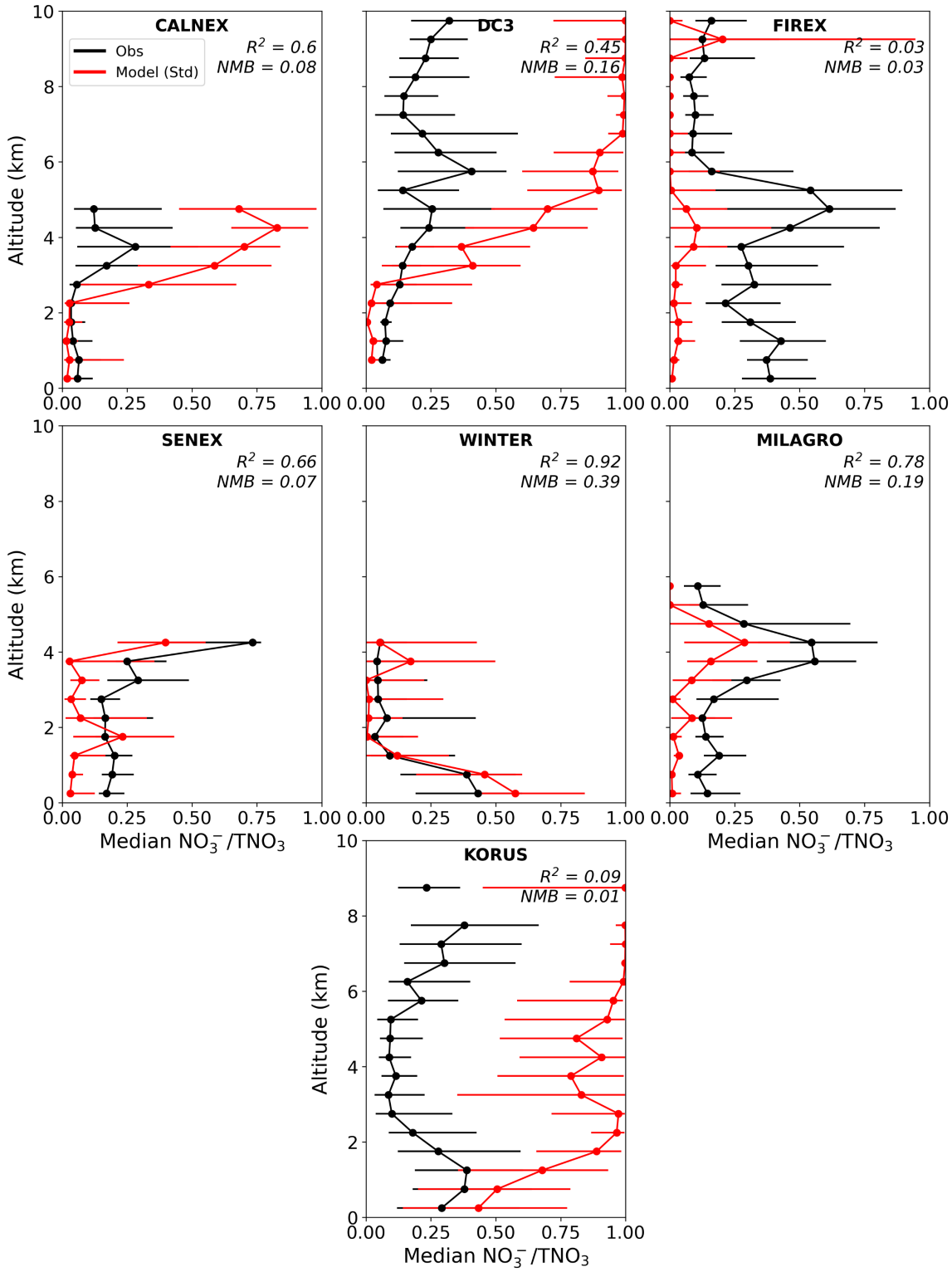

Figure S6. Median vertical profile of observed (black) and simulated (red) of the molar ratio NO_3^-/TNO_3. Points are binned to the nearest 0.5 km. Error bars represent the interquartile range (IQR). Altitude bins with less than 10 points per bin are not shown. R^2 and NMB for the vertical variability is also reported for each campaign. Points with missing or negative NO_3^- and HNO_3 are removed.

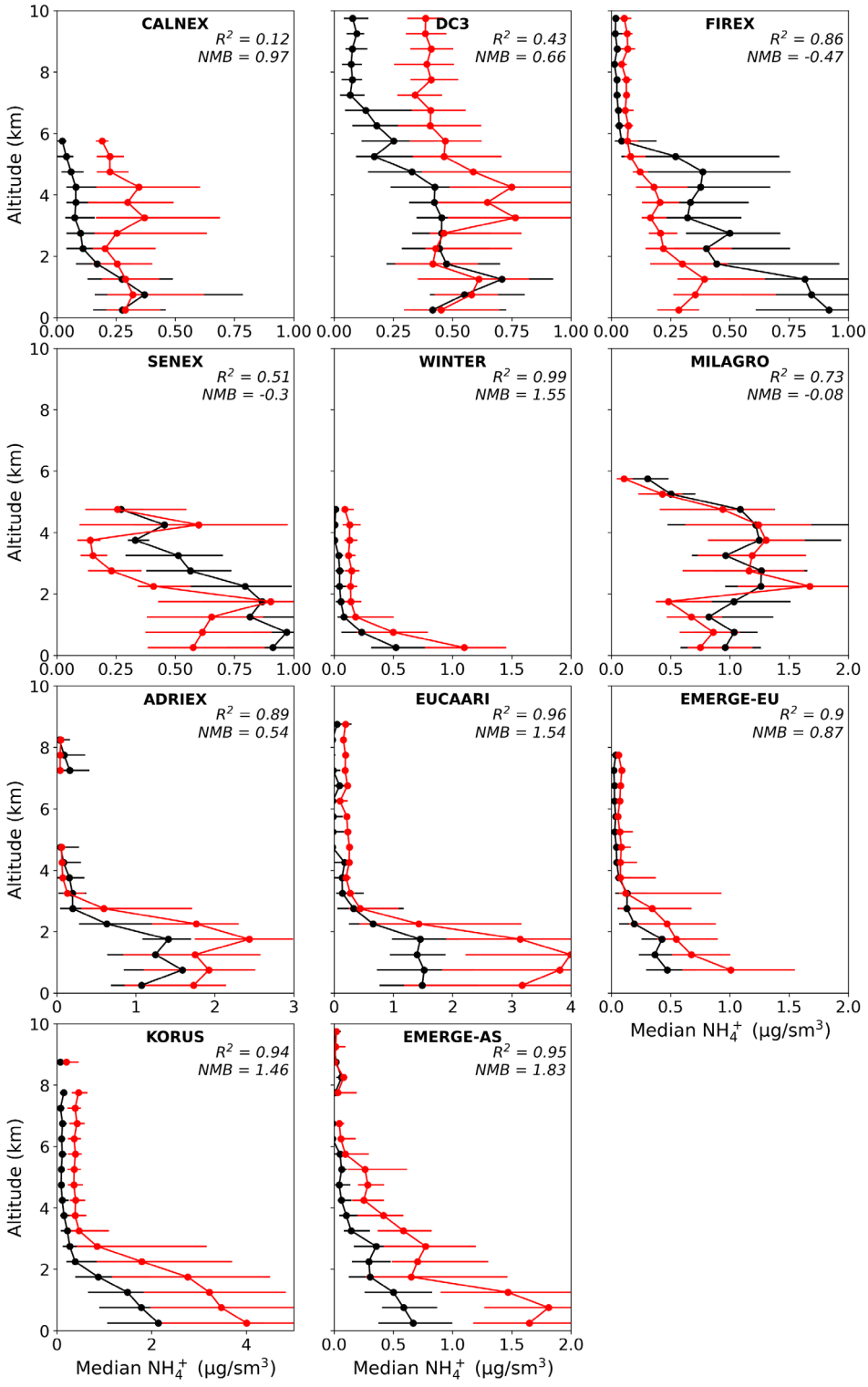

Figure S7. Median vertical profile of observed (black) and simulated (red) ammonium concentrations. Points are binned to the nearest 0.5 km. Error bars represent the interquartile range (IQR). Altitude bins with less than 10 points per bin are not shown. R^2 and NMB for the vertical variability is also reported for each campaign.

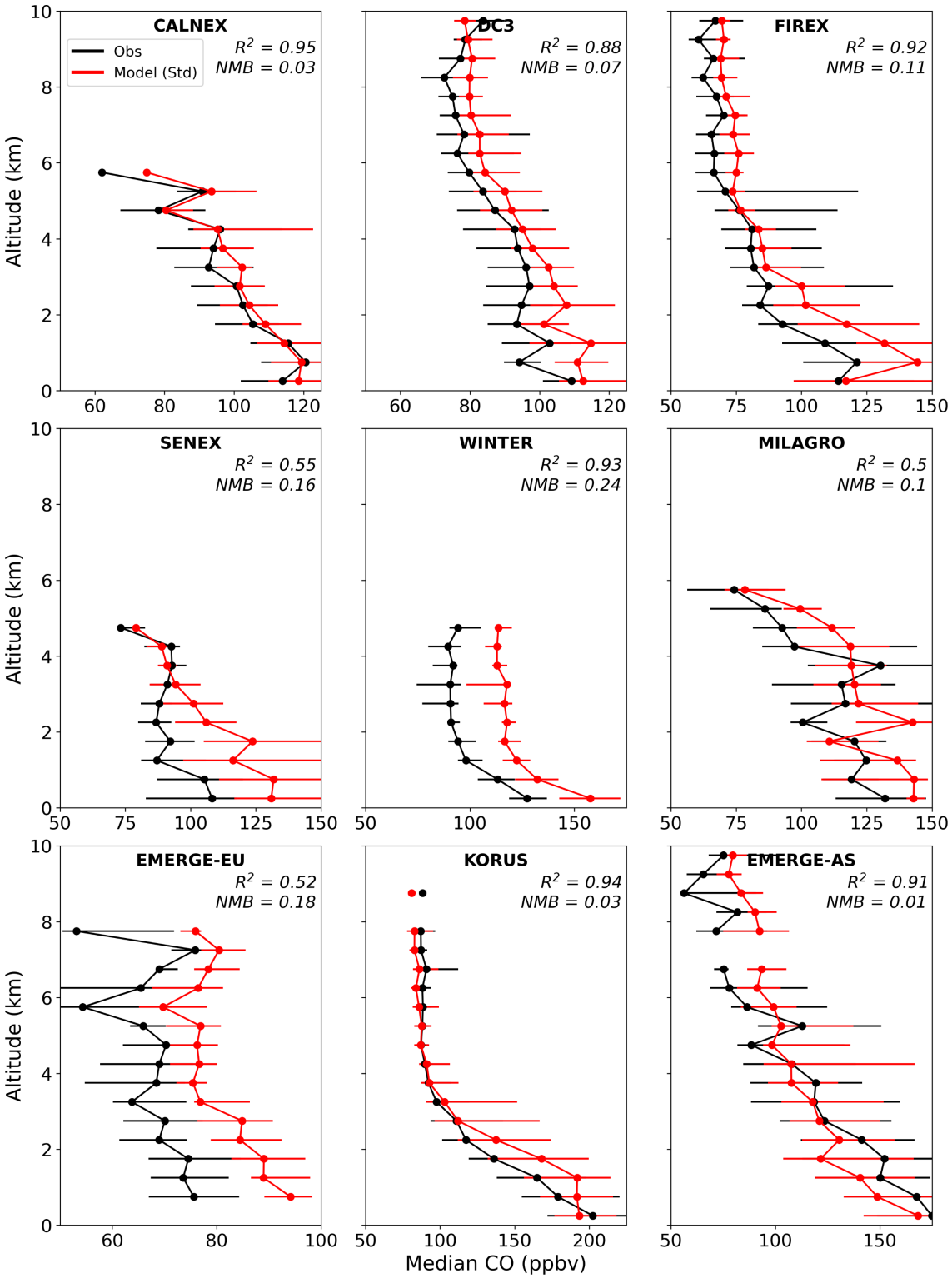

Figure S8. Median vertical profile of observed (black) and simulated (red) CO concentrations. Points are binned to the nearest 0.5 km. Error bars represent the interquartile range (IQR). Altitude bins with less than 10 points per bin are not shown. R^2 and NMB for the vertical variability is also reported for each campaign.

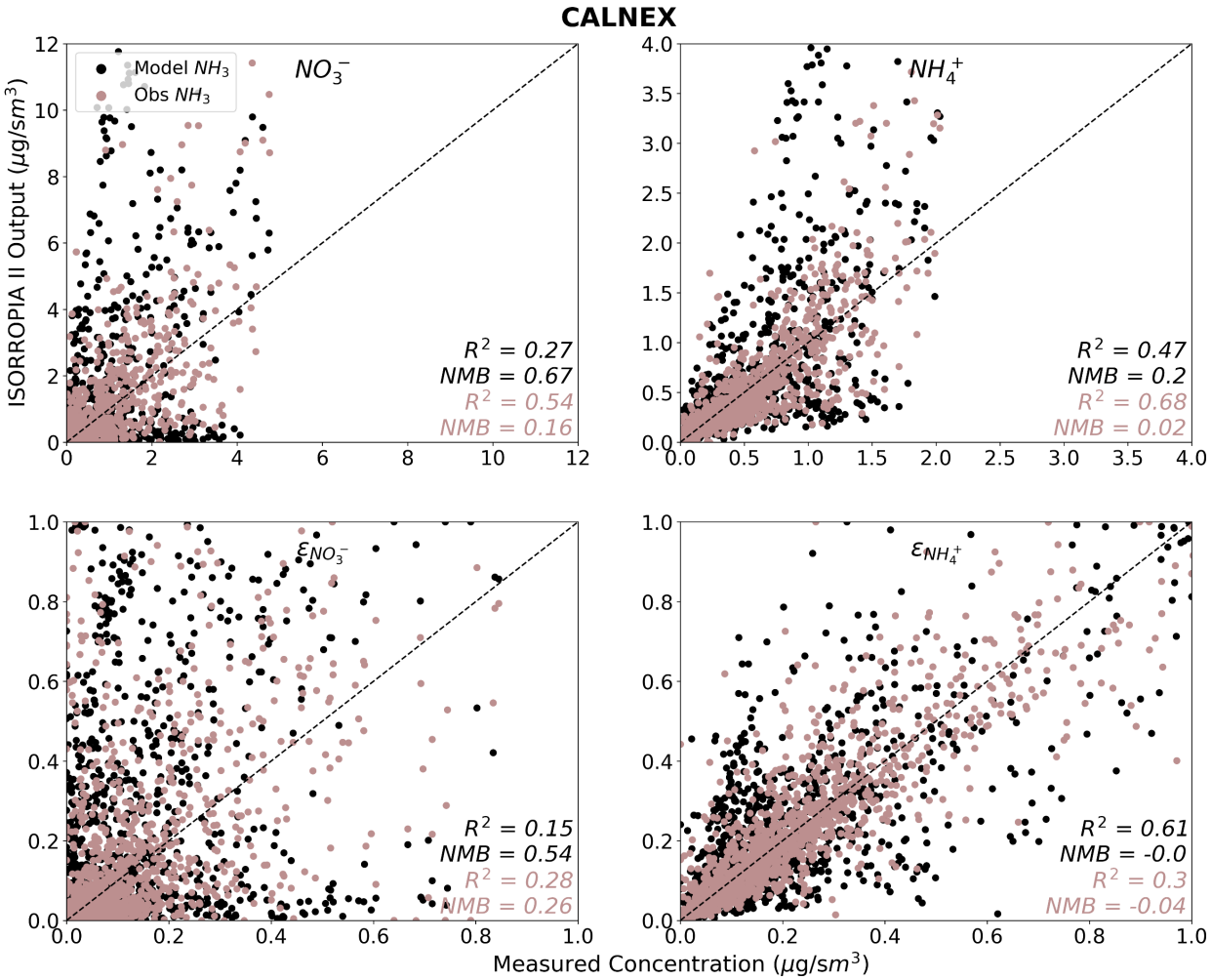

Figure S9. Comparison of the expected (x-axis) to ISORROPIA II-predicted (y-axis) NO_3^-, NH_4^+, $\varepsilon(NO_3^-)$, and $\varepsilon(NH_4^+)$ for CalNex data when model NH_3 (black) and observed NH_3 (brown) are used as input into ISORROPIA II. Observations of T, RH, SO_4^{2-}, NO_3^-, NH_4^+, HNO_3, and Cl^- are also used as inputs into ISORROPIA II. Data is filtered to retain points where model T < 300 K and 15 ≤ model RH < 90%

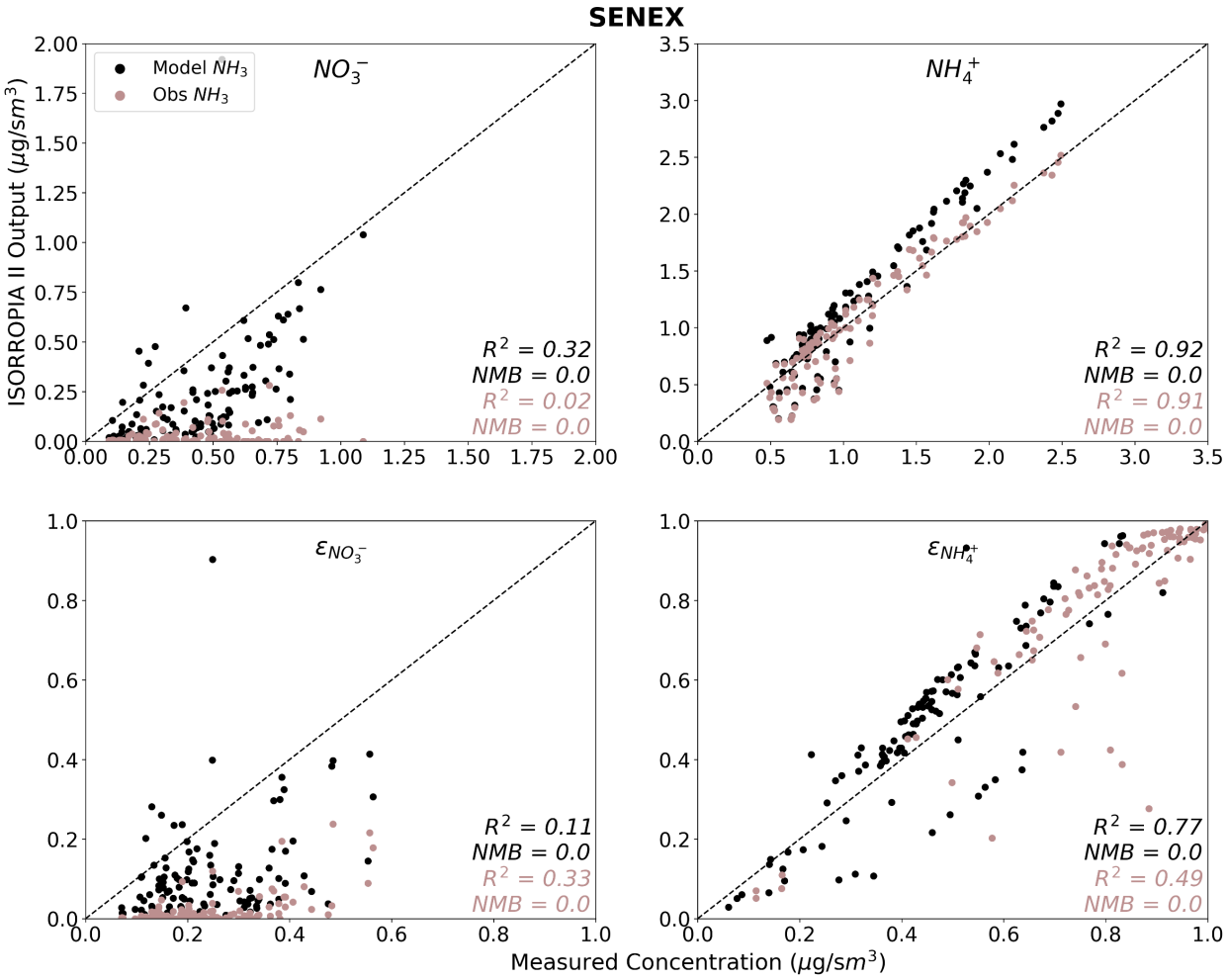

Figure S10. Comparison of the expected (x-axis) to ISORROPIA II-predicted (y-axis) NO_3^-, NH_4^+, $\varepsilon(NO_3^-)$, and $\varepsilon(NH_4^+)$ for SENEX data when model NH_3 (black) and observed NH_3 (brown) are used as input into ISORROPIA II. Observations of T, RH, SO_4^{2-}, NO_3^-, NH_4^+, HNO_3, and Cl^- are also used as inputs into ISORROPIA II. Data is filtered to retain points where model T < 300 K and 15 ≤ model RH < 90%.

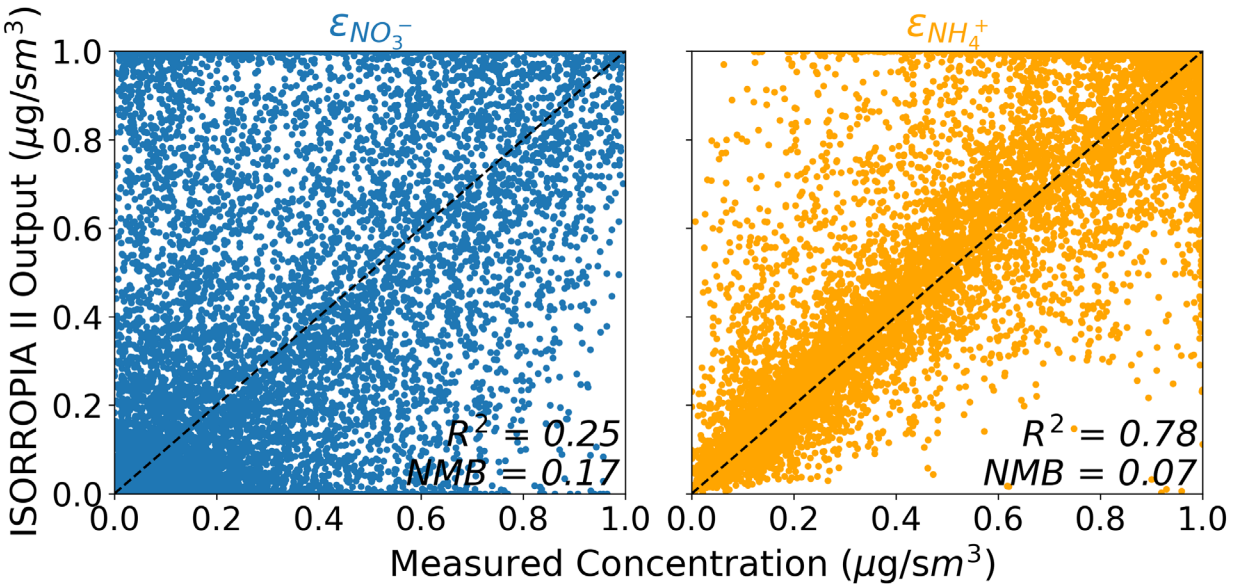

Figure S11. Comparison of the expected (x-axis) to ISORROPIA II-predicted (y-axis) $\varepsilon(NO_3^-)$ and $\varepsilon(NH_4^+)$. Observations of T, RH, SO_4^{2-}, NO_3^-, NH_4^+, HNO_3, and Cl^- are used as inputs into ISORROPIA II. Only the campaigns that made measurements of these inputs are represented. Data is filtered to retain points where model T < 300 K and 15 ≤ model RH < 90%.

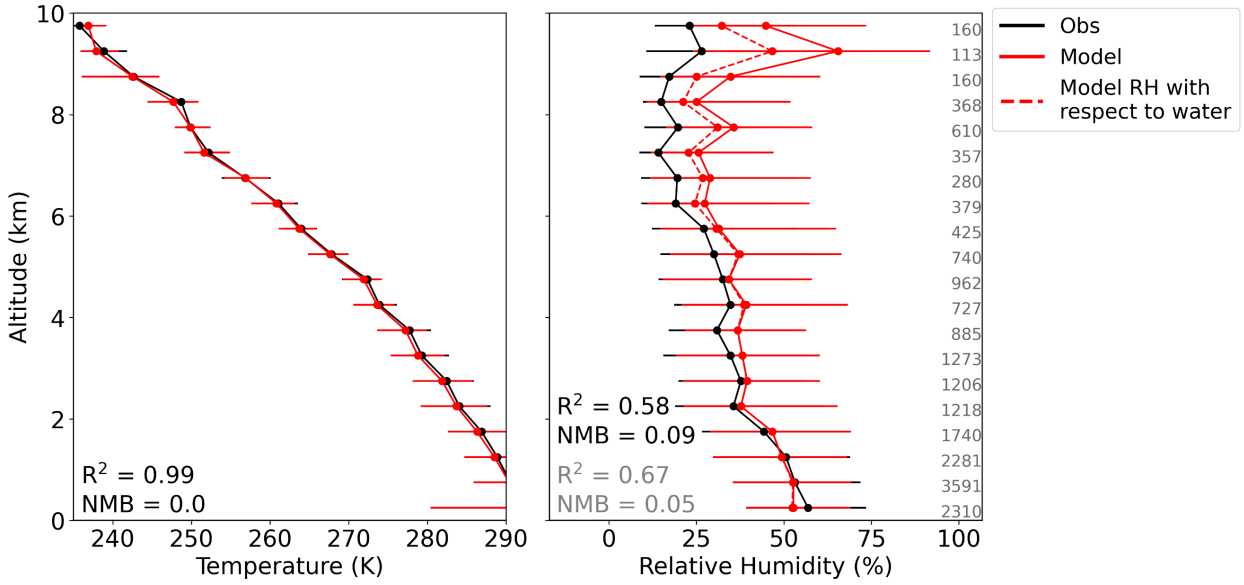

Figure S12. Temperature and RH vertical profiles for all the campaigns combined for observations (black) and model (red, solid). Model RH refers to the default RH in the model (with respect to both ice and/or water depending on the temperature). Calculated model RH with respect to only water, matching the observed RH definition, is shown with the red, dashed line. The number of points per each 0.5km altitude bin is on the right edge. R^2 and NMB are reported for each.

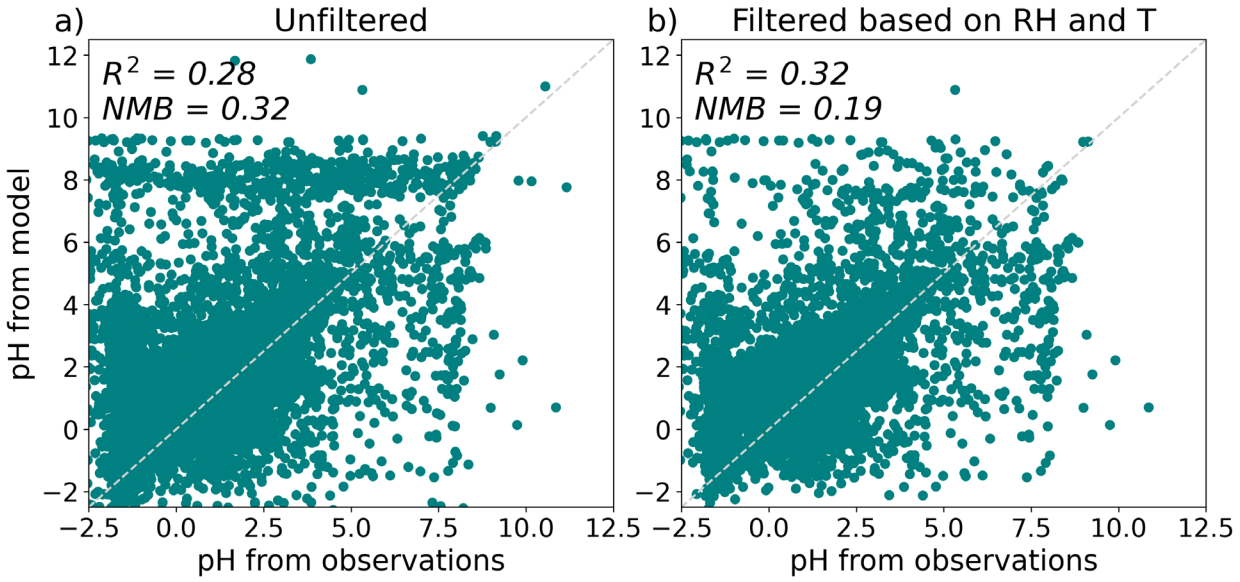

Figure S13. pH calculated using all available observed values (i.e. SNA, HNO_3, Na^+, RH, temperature, Cl^-) and using model values from GEOS-Chem as an input to standalone ISORROPIA II. Agreement between pH from observations and model is calculated a) without any filtering and b) after filtering points to remove T > 300 K and 15 ≤ RH < 90%.

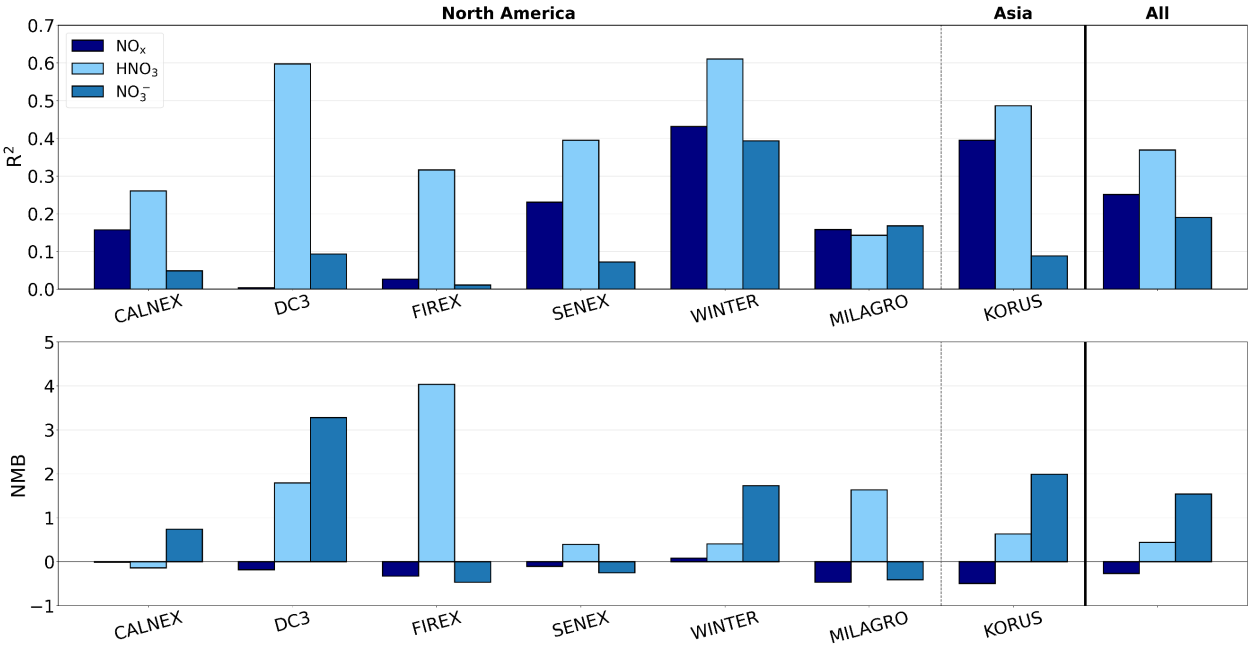

Figure S14. GEOS-Chem model performance evaluated against each airborne campaign for NO_x, HNO_3, and NO_3^- reported as R^2 and NMB. Only campaigns with that measured NO, NO_2, HNO_3, and NO_3^- are included. Campaigns are grouped by the general regions examined in this study. Model performance for all the campaigns merged into one dataset is shown under 'All'.